Generalized Gouy Rotation in a Uniform Magnetic Field

Qi Meng

Ifcen, SYSU, Zhuhai

Email: mengq8@mail2.sysu.edu.cn

April 27, 2024

Outline

Peculiar Rotation Dynamics of Electron Vortex Beams

Classically, the electron as a charged partcle, undergoes cyclotron motion in a uniform magnetic field. This can be seen from the balance of the centrifugal force against the Lorentz force:

$$\frac{m_e v^2}{r} = |e|Bv \Longrightarrow \frac{v}{r} = \frac{|e|B}{m_e} \equiv \omega_c$$

where ω_c is the cyclotron frequency.

Peculiar Rotation Dynamics of Electron Vortex Beams

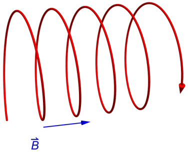

Figure: Cyclotron motion of an electron in a uniform magnetic field

Peculiar Rotation Dynamics of Electron Vortex Beams

For electron vortex beams, however, things are quite *different*! They carry *intrinsic* orbital angular momentum (OAM) and have finite size in the transverse direction, which can be characterized as a *distribution* of charge and current. The current, coiling as solenoid, generates magnetic dipole moment, which interacts with the magnetic field and gives the Zeeman energy for OAM:

$$E_{\text{Zeeman}} = -\mu_L B, \mu_L = -\frac{g_L \mu_B}{\hbar} L_z \Longrightarrow E_{\text{Zeeman}} = \frac{|e|B}{2m_e} L_z \equiv \omega_L L_z$$

where $\mu_B = \frac{\hbar|e|}{2m_e}$ is the Bohr magneton, $g_L = 1$ is the Landé g-factor for electron OAM and $\omega_L = \frac{|e|B}{2m_e} = \frac{1}{2}\omega_c$ is the Larmor frequency.

Peculiar Rotation Dynamics of Electron Vortex Beams

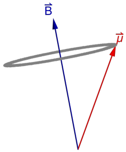

Figure: Larmor procession of electron magnetic moment in a uniform magnetic field

Peculiar Rotation Dynamics of Electron Vortex Beams

The wavefunction used to descibe the peculiar rotational dynamics of electron vortex beams in a uniform magnetic field so far has been limited to be the Landau state:

$$\Psi_{n\ell}^{\mathrm{Lan}} = A\exp(i\ell\phi) = \frac{C_{n\ell}}{w_m}\left(\frac{\sqrt{2}r}{w_m}\right)^{|\ell|} L_n^{|\ell|}\left(\frac{2r^2}{w_m^2}\right)\exp\left(-\frac{r^2}{w_m^2}\right)\exp(i\ell\phi)$$

where $w_m = 2\sqrt{\frac{\hbar}{|e|B}}$, $C_{n\ell} = \sqrt{\frac{2n!}{\pi(n+|\ell|)!}}$, n is the radial quantum number and ℓ is the azimuthal quantum number (also called topological charge), $L_n^{|\ell|}(.)$ is the generalized Laguerre polynomials.

The Landau states serve as eigenfunctions of the Hamiltonian:

$$\hat{H} = \frac{(\hat{\boldsymbol{\pi}}_\perp)^2}{2m_e} = \frac{(\hat{\boldsymbol{p}}_\perp)^2}{2m_e} + \frac{1}{2}m_e\omega_L^2 r^2 + \omega_L\hat{L}_z$$

Here, $\hat{\boldsymbol{\pi}} = \hat{\boldsymbol{p}} - e\boldsymbol{A}$ represents the kinetic momentum, with $e = -|e|$ for an electron and the symmetric gauge, expressed as $\boldsymbol{A}_S = -\frac{yB}{2}\bar{\boldsymbol{x}} + \frac{xB}{2}\bar{\boldsymbol{y}} = \frac{Br}{2}\bar{\boldsymbol{\varphi}}$ has been employed.

The corresponding eigen-energies are:

$$E = [(2n + |\ell| + 1) + \ell]\,\hbar\omega_L$$

Peculiar Rotation Dynamics of Electron Vortex Beams

Instead of rotation with a single cyclotron frequency, *the Landau electrons*, while propagating along the direction of the magnetic fields, have characteristic rotation with three different expectation value of angular velocities, depending on the eigen-value ℓ of the canonical OAM operator $\hat{L}_z = -i\frac{\partial}{\partial\varphi}$:

$$\langle\omega\rangle = \begin{cases} 0 \ (\ell < 0) \\ \omega_L \ (\ell = 0) \\ \omega_c \ (\ell > 0) \end{cases}$$

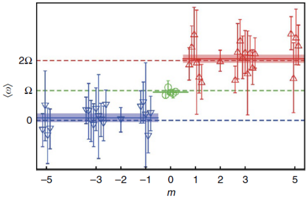

Figure: The topological-charge-dependent rotations of the vortex electron beams with the propagation distance. Figure adopted from (Schattschneider et al. 2014)

Motivation From a Review on Earlier Works

Our preliminary work develops naturally from some earlier works.

Motivation From a Review on Earlier Works

2012 — Electron Vortex Beams in a Magnetic Field: A New Twist on Landau Levels and Aharonov-Bohm States (Bliokh et al. 2012).

PHYSICAL REVIEW X **2**, 041011 (2012)

Electron Vortex Beams in a Magnetic Field: A New Twist on Landau Levels and Aharonov-Bohm States

Konstantin Y. Bliokh,[1,2] Peter Schattschneider,[3,4] Jo Verbeeck,[5] and Franco Nori[1,6]
[1]*Advanced Science Institute, RIKEN, Wako-shi, Saitama 351-0198, Japan*
[2]*A. Usikov Institute of Radiophysics and Electronics, NASU, Kharkov 61085, Ukraine*
[3]*Institut für Festkörperphysik, Technische Universität Wien, A-1040 Wien, Austria*
[4]*University Service Centre for Electron Microscopy, Technische Universität Wien, A-1040 Wien, Austria*
[5]*EMAT, University of Antwerp, Groenenborgerlaan 171, 2020 Antwerp, Belgium*
[6]*Physics Department, University of Michigan, Ann Arbor, Michigan 48109-1040, USA*
(Received 15 April 2012; published 26 November 2012)

We examine the propagation of the recently discovered electron vortex beams in a longitudinal magnetic field. We consider both the Aharonov-Bohm configuration with a single flux line and the Landau case of a uniform magnetic field. While stationary Aharonov-Bohm modes represent Bessel beams with flux- and vortex-dependent probability distributions, stationary Landau states manifest themselves as nondiffracting Laguerre-Gaussian beams. Furthermore, the Landau-state beams possess field- and vortex-dependent phases: (i) the Zeeman phase from coupling the quantized angular momentum to the magnetic field and (ii) the Gouy phase, known from optical Laguerre-Gaussian beams. Remarkably, together these phases determine the structure of Landau energy levels. This unified Zeeman-Landau-Gouy phase manifests itself in a nontrivial evolution of images formed by various superpositions of modes. We demonstrate that, depending on the chosen superposition, the image can rotate in a magnetic field with either (i) Larmor, (ii) cyclotron (double-Larmor), or (iii) zero frequency. At the same time, its centroid always follows the classical cyclotron trajectory, in agreement with the Ehrenfest theorem. Interestingly, the nonrotating superpositions reproduce stable multivortex configurations that appear in rotating superfluids. Our results open an avenue for the direct electron-microscopy observation of fundamental properties of free quantum-electron states in magnetic fields.

DOI: 10.1103/PhysRevX.2.041011 Subject Areas: Optics, Quantum Physics

Motivation From a Review on Earlier Works

- **2012** — Electron Vortex Beams in a Magnetic Field: A New Twist on Landau Levels and Aharonov-Bohm States (Bliokh et al. 2012).
- **2013** — Observation of the Larmor and Gouy Rotations with Electron Vortex Beams (Guzzinati et al. 2013).

PRL 110, 093601 (2013) PHYSICAL REVIEW LETTERS week ending 1 MARCH 2013

Observation of the Larmor and Gouy Rotations with Electron Vortex Beams

Giulio Guzzinati,[1] Peter Schattschneider,[2,3] Konstantin Y. Bliokh,[4,5] Franco Nori,[4,6] and Jo Verbeeck[1]
[1]*EMAT, University of Antwerp, Groenenborgerlaan 171, 2020 Antwerp, Belgium*
[2]*Institut für Festkörperphysik, Technische Universität Wien, A-1040 Wein, Austria*
[3]*University Service Centre for Electron Microscopy, Technische Universität Wien, A-1040 Wien, Austria*
[4]*RIKEN, Advanced Science Institute, Wako-shi, Saitama 351-0198, Japan*
[5]*A. Usikov Institute of Radiophysics and Electronics, NASU, Kharkov 61085, Ukraine*
[6]*Physics Department, University of Michigan, Ann Arbor, Michigan 48109-1040, USA*
(Received 12 November 2012; published 25 February 2013)

Electron vortex beams carrying intrinsic orbital angular momentum (OAM) are produced in electron microscopes where they are controlled and focused by using magnetic lenses. We observe various rotational phenomena arising from the interaction between the OAM and magnetic lenses. First, the Zeeman coupling, proportional to the OAM and magnetic field strength, produces an OAM-independent Larmor rotation of a mode superposition inside the lens. Second, when passing through the focal plane, the electron beam acquires an additional Gouy phase dependent on the absolute value of the OAM. This brings about the Gouy rotation of the superposition image proportional to the sign of the OAM. A combination of the Larmor and Gouy effects can result in the addition (or subtraction) of rotations, depending on the OAM sign. This behavior is unique to electron vortex beams and has no optical counterpart, as Larmor rotation occurs only for charged particles. Our experimental results are in agreement with recent theoretical predictions.

DOI: 10.1103/PhysRevLett.110.093601 PACS numbers: 42.50.Tx, 03.65.Vf, 41.85.−p

Motivation From a Review on Earlier Works

2012 · · · · · · Electron Vortex Beams in a Magnetic Field: A New Twist on Landau Levels and Aharonov-Bohm States (Bliokh et al. 2012).

2013 · · · · · · Observation of the Larmor and Gouy Rotations with Electron Vortex Beams (Guzzinati et al. 2013).

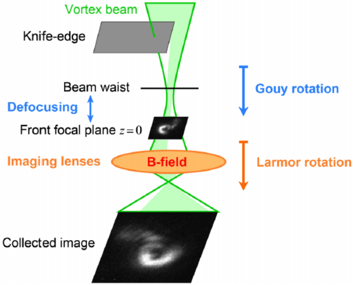

FIG. 2 (color online). (a) Schematic of the experiment. The vortex beam is prepared by using a holographic aperture in the condenser plane and then partly blocked with a knife-edge aperture. The position of the knife edge is kept fixed, whereas the beam waist position is varied (by using the condenser lens) with respect to the front focal plane of the imaging system that magnifies the image and projects it onto the CCD camera. Variations in the defocusing distance and magnification produce the Gouy and Larmor rotation effects.

Motivation From a Review on Earlier Works

2012 — Electron Vortex Beams in a Magnetic Field: A New Twist on Landau Levels and Aharonov-Bohm States (Bliokh et al. 2012).

2013 — Observation of the Larmor and Gouy Rotations with Electron Vortex Beams (Guzzinati et al. 2013).

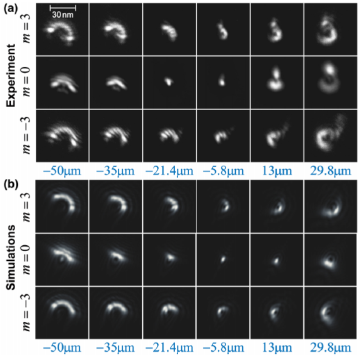

FIG. 3 (color online). Experimental imaging (a) and numerical simulations (b) of the free-space propagation of the focused truncated vortex beams (4) with $m = -3, 0, 3$ through their waist planes $z = 0$ (the defocus distance z is indicated below the panels).

Motivation From a Review on Earlier Works

2012 — Electron Vortex Beams in a Magnetic Field: A New Twist on Landau Levels and Aharonov-Bohm States (Bliokh et al. 2012).

2013 — Observation of the Larmor and Gouy Rotations with Electron Vortex Beams (Guzzinati et al. 2013).

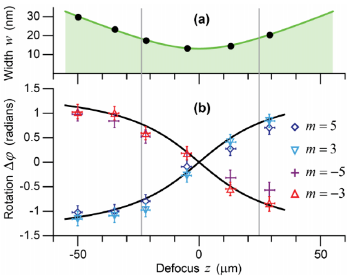

FIG. 4 (color online). Data extracted from the experimental images of Fig. 3(a). (a) The width of the $|m| = 3$ beams versus the defocus distance z. The gray lines mark $z = \pm z_R$, whereas black points indicate the planes of the measurements. (b) Angles of rotation of the C-shaped patterns (measured with respect to their orientations at $z = 0$) compared with the theoretical Gouy rotation (6) for the $m = \pm 3$ and ± 5 beams.

Motivation From a Review on Earlier Works

- **2012** — Electron Vortex Beams in a Magnetic Field: A New Twist on Landau Levels and Aharonov-Bohm States (Bliokh et al. 2012).
- **2013** — Observation of the Larmor and Gouy Rotations with Electron Vortex Beams (Guzzinati et al. 2013).
- **2014** — Imaging the dynamics of free-electron Landau states (Schattschneider et al. 2014).

nature COMMUNICATIONS

ARTICLE

Received 25 Feb 2014 | Accepted 3 Jul 2014 | Published 8 Aug 2014 DOI: 10.1038/ncomms5586 OPEN

Imaging the dynamics of free-electron Landau states

P. Schattschneider[1,2,3], Th. Schachinger[1], M. Stöger-Pollach[3], S. Löffler[3], A. Steiger-Thirsfeld[3], K.Y. Bliokh[4,5] & Franco Nori[5,6]

Landau levels and states of electrons in a magnetic field are fundamental quantum entities underlying the quantum Hall and related effects in condensed matter physics. However, the real-space properties and observation of Landau wave functions remain elusive. Here we report the real-space observation of Landau states and the internal rotational dynamics of free electrons. States with different quantum numbers are produced using nanometre-sized electron vortex beams, with a radius chosen to match the waist of the Landau states, in a quasi-uniform magnetic field. Scanning the beams along the propagation direction, we reconstruct the rotational dynamics of the Landau wave functions with angular frequency ~100 GHz. We observe that Landau modes with different azimuthal quantum numbers belong to three classes, which are characterized by rotations with zero, Larmor and cyclotron frequencies, respectively. This is in sharp contrast to the uniform cyclotron rotation of classical electrons, and in perfect agreement with recent theoretical predictions.

Motivation From a Review on Earlier Works

- **2012** Electron Vortex Beams in a Magnetic Field: A New Twist on Landau Levels and Aharonov-Bohm States (Bliokh et al. 2012).
- **2013** Observation of the Larmor and Gouy Rotations with Electron Vortex Beams (Guzzinati et al. 2013).
- **2014** Imaging the dynamics of free-electron Landau states (Schattschneider et al. 2014).

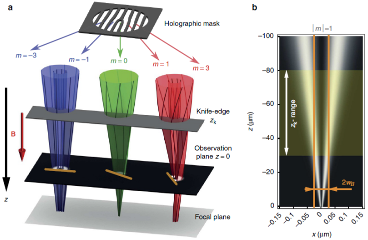

Figure 2 | Schematics of the experiment and the beam parameters. (**a**) A holographic fork mask generates a row of vortex beams with different azimuthal indices $m = ..., -5, -3, -1, 0, 1, 3, 5, ...$ (refs 19,20). These beams are focused by a magnetic lens and are studied in the region of maximal quasi-uniform magnetic field. The focal plane is shifted few Rayleigh ranges below the observation plane $z=0$ to reduce the Gouy-phase rotation[46,47]. A knife-edge stop is placed at $z_k<0$, where it blocks half of each of the beams. Varying the position z_k of the knife edge, we observe spatial rotational dynamics of the cut beams propagating to the observation plane (see Fig. 1). (**b**) Intensity distribution in the $|m|=1$ beams. The radius w of the focused beams varies slowly with z. In the highlighted range $z \in (-80, -30)$ µm, the beam radius approaches the magnetic radius, $w(z) \simeq w_B$, and the beams acquire the Landau-state properties (see Figs 3 and 4).

Motivation From a Review on Earlier Works

- **2012** Electron Vortex Beams in a Magnetic Field: A New Twist on Landau Levels and Aharonov-Bohm States (Bliokh et al. 2012).
- **2013** Observation of the Larmor and Gouy Rotations with Electron Vortex Beams (Guzzinati et al. 2013).
- **2014** Imaging the dynamics of free-electron Landau states (Schattschneider et al. 2014).

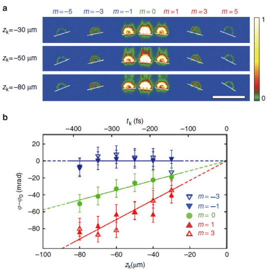

Figure 3 | Experimental images of the cut vortex beams and their *m*-dependent rotations with the propagation distance. (**a**) Experimental images of the row of the cut vortex beams with different m at different positions of the knife edge, z_k (Fig. 2). The scale bar is 50 nm. The opposite inclination of the opposite-m states is because of the residual Gouy-phase diffraction effect[46,47]. At the same time, one can see a slow rotation of the $m>0$ modes with z_k, while the $m<0$ states remain motionless. A quantitative analysis of these m-dependent rotations is depicted in **b**. The azimuthal orientations of the cut modes φ (with respect to the extrapolated reference azimuth $\varphi|_{z_k=0}=\varphi_0$) are plotted versus z_k and the corresponding timescale $t_k=z_k/v$ (on the top). Three lines correspond to the zero, Larmor and cyclotron rotations predicted for the Landau states in equation (4). Error bars include the uncertainty in reading, knife-edge roughness and stage positioning.

Motivation From a Review on Earlier Works

- **2012** — Electron Vortex Beams in a Magnetic Field: A New Twist on Landau Levels and Aharonov-Bohm States (Bliokh et al. 2012).
- **2013** — Observation of the Larmor and Gouy Rotations with Electron Vortex Beams (Guzzinati et al. 2013).
- **2014** — Imaging the dynamics of free-electron Landau states (Schattschneider et al. 2014).

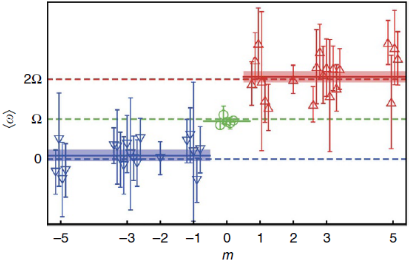

Figure 4 | Averaged rotational frequencies for modes with different azimuthal indices *m*. Averaged rotational rates $\langle \omega \rangle = v \langle d\varphi/dz_k \rangle$ (such as average slopes of the data in Fig. 3b) are shown for different topological charges m. Different data points for the same m correspond to different series of measurements, and error bars indicate the s.e.m. in each series. The solid lines represent frequencies averaged over all measurements, while the dashed lines indicate the theoretical values predicted in equation (4). The average values and s.e.m. (indicated as shaded bars) from all measurements are $\langle \omega \rangle = (0.09 \pm 0.15)\Omega$ for $m < 0$, $\langle \omega \rangle = (0.95 \pm 0.03)\Omega$ for $m = 0$ and $\langle \omega \rangle = (2.06 \pm 0.14)\Omega$ for $m > 0$. This verifies the extraordinary rotational dynamics of electrons in Landau states, which exhibit zero, Larmor and cyclotron frequencies for the modes with $m < 0$, $m = 0$ and $m > 0$, respectively.

Motivation From a Review on Earlier Works

2012 — Electron Vortex Beams in a Magnetic Field: A New Twist on Landau Levels and Aharonov-Bohm States (Bliokh et al. 2012).

2013 — Observation of the Larmor and Gouy Rotations with Electron Vortex Beams (Guzzinati et al. 2013).

2014 — Imaging the dynamics of free-electron Landau states (Schattschneider et al. 2014).

2015 — Peculiar rotation of electron vortex beams (Schachinger et al. 2015).

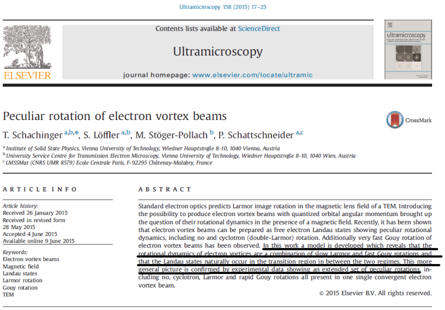
Ultramicroscopy 158 (2015) 17–25
Contents lists available at ScienceDirect
Ultramicroscopy
journal homepage: www.elsevier.com/locate/ultramic

Peculiar rotation of electron vortex beams

T. Schachinger [a,b,*], S. Löffler [a,b], M. Stöger-Pollach [b], P. Schattschneider [a,c]

[a] Institute of Solid State Physics, Vienna University of Technology, Wiedner Hauptstraße 8-10, 1040 Vienna, Austria
[b] University Service Centre for Transmission Electron Microscopy, Vienna University of Technology, Wiedner Hauptstraße 8-10, 1040 Wien, Austria
[c] LMSSMat (CNRS UMR 8579) Ecole Centrale Paris, F-92295 Châtenay-Malabry, France

ARTICLE INFO

Article history:
Received 26 January 2015
Received in revised form
28 May 2015
Accepted 4 June 2015
Available online 9 June 2015

Keywords:
Electron vortex beams
Magnetic field
Landau states
Larmor rotation
Gouy rotation
TEM

ABSTRACT

Standard electron optics predicts Larmor image rotation in the magnetic lens field of a TEM. Introducing the possibility to produce electron vortex beams with quantized orbital angular momentum brought up the question of their rotational dynamics in the presence of a magnetic field. Recently, it has been shown that electron vortex beams can be prepared as free electron Landau states showing peculiar rotational dynamics, including no and cyclotron (double-Larmor) rotation. Additionally very fast Gouy rotation of electron vortex beams has been observed. In this work a model is developed which reveals that the rotational dynamics of electron vortices are a combination of slow Larmor and fast Gouy rotations and that the Landau states naturally occur in the transition region in between the two regimes. This more general picture is confirmed by experimental data showing an extended set of peculiar rotations, including no, cyclotron, Larmor and rapid Gouy rotations all present in one single convergent electron vortex beam.

Motivation From a Review on Earlier Works

- **2012** Electron Vortex Beams in a Magnetic Field: A New Twist on Landau Levels and Aharonov-Bohm States (Bliokh et al. 2012).
- **2013** Observation of the Larmor and Gouy Rotations with Electron Vortex Beams (Guzzinati et al. 2013).
- **2014** Imaging the dynamics of free-electron Landau states (Schattschneider et al. 2014).
- **2015** Peculiar rotation of electron vortex beams (Schachinger et al. 2015).

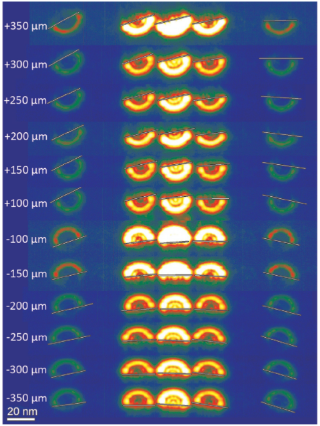

Fig. 3. Experimental images of cut EVBs of a z-shift series. The non-overlapping vortex orders |m| = 0, 1, 3 are visible. The measured azimuthal rotation angle is inidcated as a faint solid line. Rotational dynamics can be observed by eye for all vortex orders. (For interpretation of the references to color in this figure caption, the reader is referred to the web version of this paper.)

Motivation From a Review on Earlier Works

2012 Electron Vortex Beams in a Magnetic Field: A New Twist on Landau Levels and Aharonov-Bohm States (Bliokh et al. 2012).

2013 Observation of the Larmor and Gouy Rotations with Electron Vortex Beams (Guzzinati et al. 2013).

2014 Imaging the dynamics of free-electron Landau states (Schattschneider et al. 2014).

2015 Peculiar rotation of electron vortex beams (Schachinger et al. 2015).

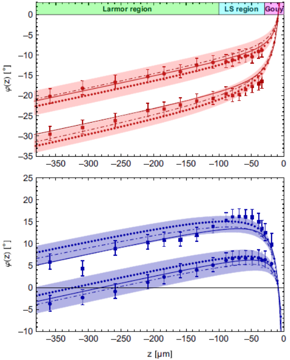

Fig. 4. Experimental data (large dots with error bars, $|m| = 1$, squares $|m| = 3$, upper diagram, red, $m > 0$, lower diagram, blue, $m < 0$) giving the azimuthal rotation angle $\varphi(z)$ of the cut EVBs over the z-shift value for an experiment scanning the LR- and LS-region. Eq. (23) was used to calculate the small dots using moments from the numerical simulation. For the solid lines, moments from the DLG modes, Eq. (14), were taken, using $z_R = 1.46$ μm for $|m| = 1$ and $z_R = 2.84$ μm for $|m| = 3$. The dot dashed lines show the influence of 35% symmetric OAM impurities applied to the pure numerical simulated vortices using Eq. (33), whereas the shaded areas indicate solely asymmetric OAM impurity contributions of 17.5%. Error bars include the estimated reading error, knife-edge roughness and stage positioning. (For interpretation of the references to color in this figure caption, the reader is referred to the web version of this paper.)

Motivation From a Review on Earlier Works

- **2012** — Electron Vortex Beams in a Magnetic Field: A New Twist on Landau Levels and Aharonov-Bohm States (Bliokh et al. 2012).
- **2013** — Observation of the Larmor and Gouy Rotations with Electron Vortex Beams (Guzzinati et al. 2013).
- **2014** — Imaging the dynamics of free-electron Landau states (Schattschneider et al. 2014).
- **2015** — Peculiar rotation of electron vortex beams (Schachinger et al. 2015).
- **2021** — General quantum-mechanical solution for twisted electrons in a uniform magnetic field (Zou, Zhang, and Silenko 2021).

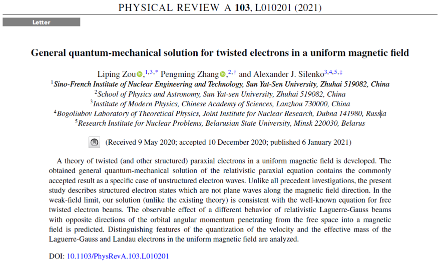
PHYSICAL REVIEW A **103**, L010201 (2021)

Letter

General quantum-mechanical solution for twisted electrons in a uniform magnetic field

Liping Zou,[1,3,*] Pengming Zhang,[2,†] and Alexander J. Silenko[3,4,5,‡]
[1]*Sino-French Institute of Nuclear Engineering and Technology, Sun Yat-Sen University, Zhuhai 519082, China*
[2]*School of Physics and Astronomy, Sun Yat-sen University, Zhuhai 519082, China*
[3]*Institute of Modern Physics, Chinese Academy of Sciences, Lanzhou 730000, China*
[4]*Bogoliubov Laboratory of Theoretical Physics, Joint Institute for Nuclear Research, Dubna 141980, Russia*
[5]*Research Institute for Nuclear Problems, Belarusian State University, Minsk 220030, Belarus*

(Received 9 May 2020; accepted 10 December 2020; published 6 January 2021)

A theory of twisted (and other structured) paraxial electrons in a uniform magnetic field is developed. The obtained general quantum-mechanical solution of the relativistic paraxial equation contains the commonly accepted result as a specific case of unstructured electron waves. Unlike all precedent investigations, the present study describes structured electron states which are not plane waves along the magnetic field direction. In the weak-field limit, our solution (unlike the existing theory) is consistent with the well-known equation for free twisted electron beams. The observable effect of a different behavior of relativistic Laguerre-Gauss beams with opposite directions of the orbital angular momentum penetrating from the free space into a magnetic field is predicted. Distinguishing features of the quantization of the velocity and the effective mass of the Laguerre-Gauss and Landau electrons in the uniform magnetic field are analyzed.

DOI: 10.1103/PhysRevA.103.L010201

Motivation From a Review on Earlier Works

2012 — Electron Vortex Beams in a Magnetic Field: A New Twist on Landau Levels and Aharonov-Bohm States (Bliokh et al. 2012).

2013 — Observation of the Larmor and Gouy Rotations with Electron Vortex Beams (Guzzinati et al. 2013).

2014 — Imaging the dynamics of free-electron Landau states (Schattschneider et al. 2014).

2015 — Peculiar rotation of electron vortex beams (Schachinger et al. 2015).

2021 — General quantum-mechanical solution for twisted electrons in a uniform magnetic field (Zou, Zhang, and Silenko 2021).

Advanced results obtained in optics allow us to rigorously derive a general formula for the paraxial wave function of a relativistic twisted Dirac particle in a uniform magnetic field. In this case, the exact relativistic FW Hamiltonian is given by [25,39–41]

$$i\frac{\partial\Psi_{\mathrm{FW}}}{\partial t}=\mathcal{H}_{\mathrm{FW}}\Psi_{\mathrm{FW}},\quad \mathcal{H}_{\mathrm{FW}}=\beta\sqrt{m^2+\pi^2-e\boldsymbol{\Sigma}\cdot\boldsymbol{B}},\quad (7)$$

where $\pi=p-eA$ is the kinetic momentum and β and Σ are the Dirac matrices. This Hamiltonian acts on the bispinor $\Psi_{\mathrm{FW}}=\binom{\Phi_{\mathrm{FW}}}{0}$. The zero lower spinor of the bispinor can be disregarded. Eigenfunctions (more precisely, an upper spinor) of the *relativistic* FW Hamiltonian coincide with the *nonrelativistic* Landau solution (2) because the operator $\pi^2-e\boldsymbol{\Sigma}\cdot\boldsymbol{B}$ commutes with the Hamiltonian in both cases (see Refs. [25,39,40]). The FW representation is important for obtaining a classical limit of relativistic quantum mechanics [42] and establishing a connection between relativistic and nonrelativistic quantum mechanics [43,44].

Let us denote $P=\sqrt{E^2-m^2}=\hbar k$, where E is an energy of a stationary state. A transformation of Hamiltonian equations in the FW representation to the paraxial form has been considered in Refs. [28,31,45]. Squaring Eq. (7) for the upper spinor, applying the paraxial approximation for $p_z>0$, and the substitution $\Phi_{\mathrm{FW}}=\exp(ikz)\Psi$ lead to the paraxial equation [45]

$$\left(\nabla_\perp^2-ieB\frac{\partial}{\partial\phi}-\frac{e^2B^2r^2}{4}+2es_zB+2ik\frac{\partial}{\partial z}\right)\Psi=0,\quad (8)$$

where s_z is the spin projection onto the field direction. The above-mentioned substitution is equivalent to shifts of the zero energy level and of the squared particle momentum in Schrödinger quantum mechanics. When $B=0$, Eq. (8) takes the form of the paraxial wave equation for free electrons (4).

Motivation From a Review on Earlier Works

- **2012** — Electron Vortex Beams in a Magnetic Field: A New Twist on Landau Levels and Aharonov-Bohm States (Bliokh et al. 2012).
- **2013** — Observation of the Larmor and Gouy Rotations with Electron Vortex Beams (Guzzinati et al. 2013).
- **2014** — Imaging the dynamics of free-electron Landau states (Schattschneider et al. 2014).
- **2015** — Peculiar rotation of electron vortex beams (Schachinger et al. 2015).
- **2021** — General quantum-mechanical solution for twisted electrons in a uniform magnetic field (Zou, Zhang, and Silenko 2021).

The straightforward solution of these differential equations is based on known integrals [50] and has the form (Supplemental Material [49], Sec. II)

$$
\begin{aligned}
w(z) &= w_0\sqrt{\frac{1}{2}\left[1+\frac{w_m^4}{w_0^4}-\left(\frac{w_m^4}{w_0^4}-1\right)\cos\frac{2z}{z_m}\right]}\\
&= w_0\sqrt{\cos^2\frac{z}{z_m}+\frac{w_m^4}{w_0^4}\sin^2\frac{z}{z_m}}, \quad z_m=\frac{kw_m^2}{2},\\
R(z) &= kw_m^2\frac{\cos^2\frac{z}{z_m}+\frac{w_m^4}{w_0^4}\sin^2\frac{z}{z_m}}{\left(\frac{w_m^4}{w_0^4}-1\right)\sin\frac{2z}{z_m}},\\
\Phi_G(z) &= N\arctan\left(\frac{w_m^2}{w_0^2}\tan\frac{z}{z_m}\right)+\frac{(\ell+2s_z)z}{z_m}.
\end{aligned} \tag{13}
$$

The normalization constant $C_{n\ell}$ is given by Eq. (2).

So far, the study on rotational behaviour of the vortex electron beam in uniform magnetic field uses the Landau states, which has a constant beam width.

But the experiment done in (Schachinger et al. 2015) suggest that at a larger length scale, where the beam width changes as propagting in the magnetic field, some new candidates for electron vortex beam is anticipated.

Luckily, we are armed with such a new vortex beam wavefunction, as proposed in (Zou, Zhang, and Silenko 2021). Now it is worth trying to reexamine the rotational dynamics of the electron vortex beam.

This is one of the main efforts done in our ready-to-come work.

Before going any further, we take a closer look at the paraxial Landau modes, which is the main

Both the free Laguerre-Gaussian (LG) beams and paraxial Landau modes are described by the following familiar form:

$$\Psi_{n\ell}(r,\varphi,z) = A\exp(i\ell\varphi)\exp\left[i\frac{kr^2}{2R(z)}\right]\exp\left[-i\Phi_G(z)\right],$$
$$A = \frac{C_{n\ell}}{w(z)}\left(\frac{\sqrt{2}r}{w(z)}\right)^{|\ell|} L_n^{|\ell|}\left(\frac{2r^2}{w(z)^2}\right)\exp\left(-\frac{r^2}{w(z)^2}\right), \tag{1}$$
$$C_{n\ell} = \sqrt{\frac{2n!}{\pi(n+|\ell|)!}},$$

Note that the Landau states do not have the terms $\exp\left[i\frac{kr^2}{2R(z)}\right]\exp\left[-i\Phi_G(z)\right]$.

Function	Free beams	Paraxial Landau modes
$w(z)$	$w_0\sqrt{1+\frac{z^2}{z_R^2}}$	$w_0\sqrt{\cos^2\frac{z}{z_m}+\frac{z_m^2}{z_R^2}\sin^2\frac{z}{z_m}}$
$R(z)$	$z+\frac{z_R^2}{z}$	$kw_m^2\frac{\cos^2\frac{z}{z_m}+\frac{z_m^2}{z_R^2}\sin^2\frac{z}{z_m}}{\left(\frac{z_m^2}{z_R^2}-1\right)\sin\frac{2z}{z_m}}$
$\Phi_G(z)$	$(2n+\lvert\ell\rvert+1)\arctan(\frac{z}{z_R})$	$(2n+\lvert\ell\rvert+1)\arctan\left(\frac{z_m}{z_R}\tan\frac{z}{z_m}\right)+\ell\frac{z}{z_m}$

where the beam waist w_0 and the magnetic length parameter $w_m=2\sqrt{\frac{\hbar}{|e|B}}$ are the characteristic transverse length scales and $z_R=\frac{1}{2}kw_0^2$ and $z_m=\frac{1}{2}kw_m^2$ are the characteristic longitudinal length scales for the free beams and paraxial Landau modes separately.

Note that the paraxial Landau modes coincides with the Landau state except for an additional Gouy phase if $w_0=w_m$, and can degenerate to the free beam for $B\to 0$.

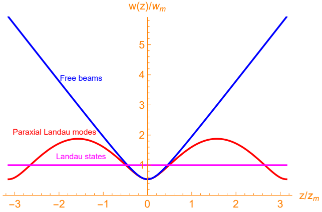

Figure: The beam width $w(z)$ of the free beams, the Landau states and the paraxial Landau modes

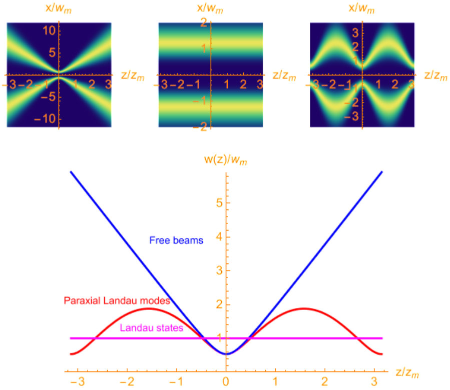

Figure: From left to right, the free beams, the Landau states and the paraxial Landau modes

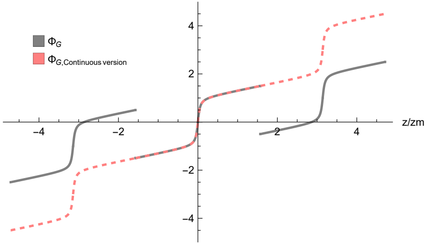

Figure: Gouy phase of paraxial Landau modes and its continuous version

For the Gouy phase $\Phi_G(z)$ of paraxial Landau modes, it could be understood as the continuous version:

$$\Phi_G(z) = (2n + |\ell| + 1)\left(\arctan\left(\frac{z_m}{z_R}\tan\frac{z}{z_m}\right) + \pi\left\lfloor\frac{z}{\pi z_m} + \frac{1}{2}\right\rfloor\right) + \ell\frac{z}{z_m}, \qquad (2)$$

where $\lfloor . \rfloor$ is the floor function.

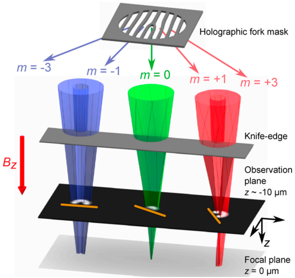

Figure: Experiment Setup in (Schattschneider et al. 2014; Schachinger et al. 2015) for observing the internal rotational dynamics inside the cylindrically symmetric beams. Figure adopted from (Schattschneider et al. 2014)

After introducing the paraxial Landau modes, we now pass to the experiment that our model aims to explain.

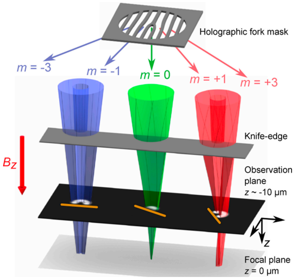

Figure: Experiment Setup in (Schattschneider et al. 2014; Schachinger et al. 2015) for observing the internal rotational dynamics inside the cylindrically symmetric beams. Figure adopted from (Schattschneider et al. 2014)

- The convergent electron vortex beams enter the longitudinal magnetic field B_z of the objective lens and are incident on a knife-edge (KE). The electron vortex beams cutted by the KE will propagate down the column and reach the observation plane
- Adjusting the position of the KE allows for measuring the rotational dynamics of EVBs, observed as variations in the azimuthal angle of the intensity patterns

- The rotation of electron vortex beams in a magnetic field is closely linked to the Bohmian trajectories.

- The rotation of electron vortex beams in a magnetic field is closely linked to the Bohmian trajectories.
- Specifically, these trajectories illustrate the spiraling motion of electrons around the magnetic-field direction.

- The rotation of electron vortex beams in a magnetic field is closely linked to the Bohmian trajectories.
- Specifically, these trajectories illustrate the spiraling motion of electrons around the magnetic-field direction.
- In this context, the angular velocity of the electron as a quantum fluid along the streamlines of the probability current is defined to be $\omega(r) = \frac{v_\varphi(r)}{r}$ (where $\boldsymbol{v} = \boldsymbol{j}/\rho$ is the local Bohmian velocity, i.e. the velocity on a streamline and $\boldsymbol{j}$ is the gauge-invariant probability current, ρ is the probability density).

- The rotation of electron vortex beams in a magnetic field is closely linked to the Bohmian trajectories.
- Specifically, these trajectories illustrate the spiraling motion of electrons around the magnetic-field direction.
- In this context, the angular velocity of the electron as a quantum fluid along the streamlines of the probability current is defined to be $\omega(r) = \frac{v_\varphi(r)}{r}$ (where $\boldsymbol{v} = \boldsymbol{j}/\rho$ is the local Bohmian velocity, i.e. the velocity on a streamline and $\boldsymbol{j}$ is the gauge-invariant probability current, ρ is the probability density).
- The expectation value of this angular velocity turns out to be $\langle\omega\rangle(z) = \omega_L \left(\text{sgn}(\ell)\frac{w_m^2}{w(z)^2} + 1\right)$, where $\text{sgn}(.)$ is the sign function, ω_L is the Larmor frequency.

- The expectation value of this angular velocity turns out to be $\langle\omega\rangle(z) = \omega_L\left(\text{sgn}(\ell)\frac{w_m^2}{w(z)^2}+1\right)$, where $\mathrm{sgn}(.)$ is the sign function, ω_L is the Larmor frequency.
- For Landau states, $w(z) = w_m$, we then have the famous splitting of three frequencies:

$$\langle\omega\rangle(z) = \omega_L\left(\text{sgn}(\ell)+1\right)$$

- Assuming uniform motion in z-direction $z \simeq vt$, $\langle \omega \rangle = \frac{d\langle \varphi \rangle}{dt} \simeq v \frac{d\langle \varphi \rangle}{dz}$.

- Assuming uniform motion in z-direction $z \simeq vt$, $\langle \omega \rangle = \frac{d\langle \varphi \rangle}{dt} \simeq v \frac{d\langle \varphi \rangle}{dz}$.
- We can then calculated the Bohmian rotation angle using the $w(z)$ of paraxial Landau modes:

$$\begin{aligned} \langle \varphi \rangle &= \frac{1}{v} \int \langle \omega \rangle \, dz \\ &= \frac{z}{z_m} + \mathsf{sgn}\ (\ell) \arctan\left(\frac{z_m}{z_R} \tan\left(\frac{z}{z_m} \right) \right) \end{aligned} \tag{3}$$

- Assuming uniform motion in z-direction $z \simeq vt$, $\langle\omega\rangle = \frac{d\langle\varphi\rangle}{dt} \simeq v\frac{d\langle\varphi\rangle}{dz}$.
- We can then calculated the Bohmian rotation angle using the $w(z)$ of paraxial Landau modes:

$$\begin{aligned}\langle\varphi\rangle &= \frac{1}{v}\int\langle\omega\rangle\, dz \\ &= \frac{z}{z_m} + \mathrm{sgn}\,(\ell)\arctan\left(\frac{z_m}{z_R}\tan\left(\frac{z}{z_m}\right)\right)\end{aligned} \tag{3}$$

- Recall that for paraxial Landau modes the Gouy phase reads:

$$\Phi_G = (2n + |\ell| + 1)\arctan\left(\frac{z_m}{z_R}\tan\frac{z}{z_m}\right) + \ell\frac{z}{z_m} \tag{4}$$

- Assuming uniform motion in z-direction $z \simeq vt$, $\langle\omega\rangle = \frac{d\langle\varphi\rangle}{dt} \simeq v\frac{d\langle\varphi\rangle}{dz}$.
- We can then calculated the Bohmian rotation angle using the $w(z)$ of paraxial Landau modes:

$$\begin{aligned}\langle\varphi\rangle &= \frac{1}{v}\int\langle\omega\rangle\, dz \\ &= \frac{z}{z_m} + \mathsf{sgn}\,(\ell)\arctan\left(\frac{z_m}{z_R}\tan\left(\frac{z}{z_m}\right)\right)\end{aligned} \tag{3}$$

- Recall that for paraxial Landau modes the Gouy phase reads:

$$\Phi_G = (2n + |\ell| + 1)\arctan\left(\frac{z_m}{z_R}\tan\frac{z}{z_m}\right) + \ell\frac{z}{z_m} \tag{4}$$

- Thus, the Bohmian rotation angle in a uniform field can be characterized by the Gouy phase of the paraxial Landau modes.

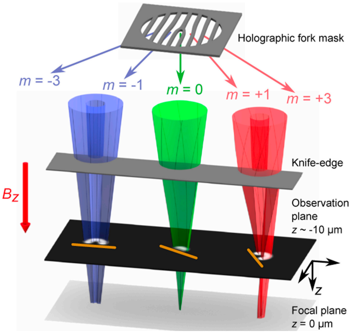

Figure: Experiment Setup. Figure adopted from (Schattschneider et al. 2014)

- The measured angle in the experiment is the angle difference between the knife-edge cutting position z_k and the observation plane position z_{df}.

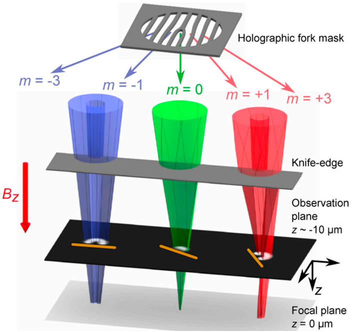

Figure: Experiment Setup. Figure adopted from (Schattschneider et al. 2014)

- The measured angle in the experiment is the angle difference between the knife-edge cutting position z_k and the observation plane position z_{df}.
- Based on paraxial Landau modes, we can analytically calculate this observable:

$$\Delta\langle\phi\rangle = \frac{z - z_{df}}{z_m} + \mathrm{sgn}\,(\ell)\left[\arctan\left(\frac{z_m}{z_R}\tan\left(\frac{z}{z_m}\right)\right) - \arctan\left(\frac{z_m}{z_R}\tan\left(\frac{z_{df}}{z_m}\right)\right)\right] \tag{5}$$

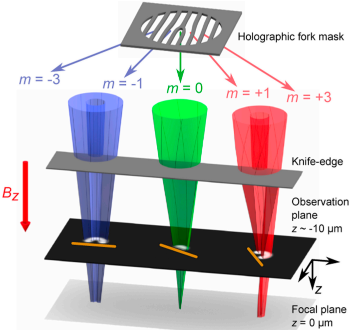

Figure: Experiment Setup. Figure adopted from (Schattschneider et al. 2014)

- The measured angle in the experiment is the angle difference between the knife-edge cutting position z_k and the observation plane position z_{df}.
- Based on paraxial Landau modes, we can analytically calculate this observable:

$$\Delta\langle\phi\rangle = \frac{z - z_{df}}{z_m} + \operatorname{sgn}(\ell)\left[\arctan\left(\frac{z_m}{z_R}\tan\left(\frac{z}{z_m}\right)\right) - \arctan\left(\frac{z_m}{z_R}\tan\left(\frac{z_{df}}{z_m}\right)\right)\right] \quad (5)$$

- This formula is the model that we will use to explain the experimental data.

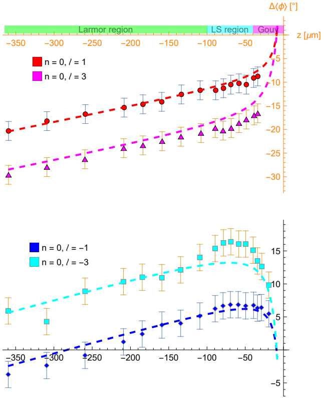

Figure: Prediction of experimental data in (Schachinger et al. 2015)

- In the work (Schachinger et al. 2015), they used $w(z) = w_0\sqrt{1+\frac{z^2}{z_R^2}}$ of free beams in

$$\langle\omega\rangle(z) = \omega_L\left(\text{sgn}(\ell)\frac{w_m^2}{w(z)^2}+1\right)$$

 as an approximation for the beam width in their experimental setup and gets a good result, as can be seen in the figure on the left, where the dashed lines are the predicting curves and n, ℓ are quantum numbers label the LG modes.
- Based on the different rotational behaviours, they divided the z axis in three regions: Gouy, Landau state (LS), and Larmor.
- For the Landau state region, it refers to the beam width $w(z) \approx w_m$.

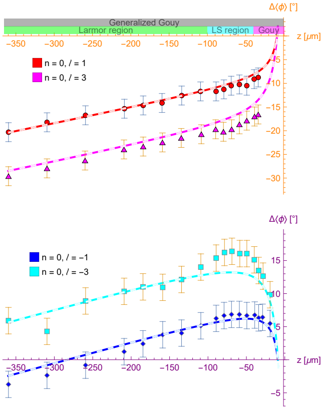

Figure: Predictions of experimental data in (Schachinger et al. 2015)

In our work, we explain the experimental data with the paraxial Landau modes, using the experimental parameters.

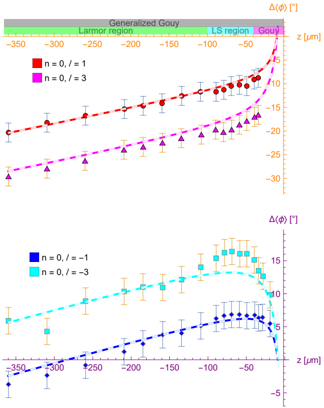

Figure: Predictions of experimental data in (Schachinger et al. 2015)

As can be seen, the two fitting curves almost coincide under the experimental parameters, of difference only $\sim 0.001°$.

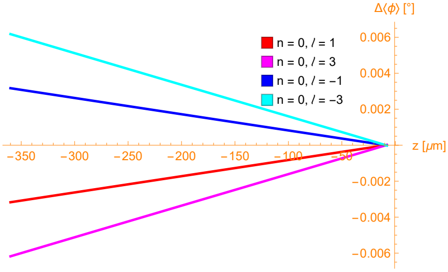

Figure: The differences between the predicting curves based on paraxial Landau modes and based on free beams

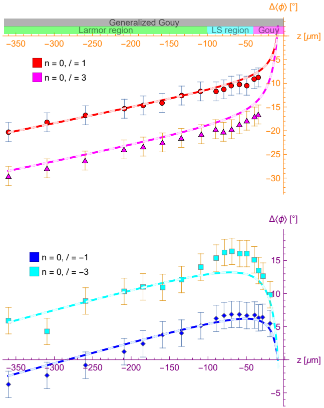

Figure: Predictions of experimental data in (Schachinger et al. 2015)

This is due to the fact that in the range of interest of z and under the parameters in this experiment, the free beam width and the paraxial Landau modes beam width are very close to each other.

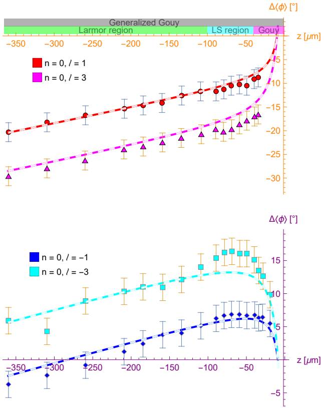

Figure: Predictions of experimental data in (Schachinger et al. 2015)

Since all the contribution comes from the Gouy phase term of the paraxial Landau modes, We can unify the whole propagtion region as the Generalized Gouy.

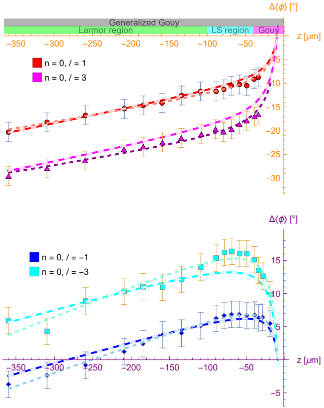

Figure: Prediction of experimental data in (Schachinger et al. 2015)

If we choose some parameters other than that of the experimental for the model:

$$\Delta\langle\phi\rangle = \frac{z - z_{df}}{z_m} + \operatorname{sgn}(\ell)\left[\arctan\left(\frac{z_m}{z_R}\tan\left(\frac{z}{z_m}\right)\right) - \arctan\left(\frac{z_m}{z_R}\tan\left(\frac{z_{df}}{z_m}\right)\right)\right]$$

with z_m, z_R as parameters, we can get a very good approximation of the experimental data.

Table: Parameters used in the experiment and in best approximation

modes	Experimental (z_R, z_m)	Best approximation (z_R, z_m)
$n = 0, \ell = -3$	$(2.84, 1760)$	$(3.46, 1200)$
$n = 0, \ell = -1$	$(1.46, 1760)$	$(1.65, 1381)$
$n = 0, \ell = 1$	$(1.46, 1760)$	$(1.68, 2129)$
$n = 0, \ell = 3$	$(2.84, 1760)$	$(3.38, 2274)$

The paraxial equation for twisted electron beam in uniform magnetic field:

$$\left[2i\hbar^2 k\frac{\partial}{\partial z} + \hbar^2\nabla_\perp^2 - i\hbar eB\frac{\partial}{\partial\varphi} - \frac{1}{4}e^2B^2r^2\right]\Psi = 0 \tag{6}$$

Note that for uniform motion in z-directioon, $z \approx vt$, Eq.(6) is equivalent to the time-dependent Schrödinger equation (TDSE):

$$\begin{aligned} i\hbar\frac{\partial}{\partial z} &= -\frac{\hbar}{2k}\nabla_\perp^2 + i\frac{eB}{2k}\frac{\partial}{\partial\varphi} + \frac{e^2B^2r^2}{8\hbar k} \\ \overset{z\approx vt}{\Longrightarrow} i\hbar\frac{\partial}{\partial t} &= -\frac{\hbar^2}{2m_e}\nabla_\perp^2 + i\frac{\hbar eB}{2m_e}\frac{\partial}{\partial\varphi} + \frac{e^2B^2r^2}{8m_e} \\ &= \frac{\hat{\boldsymbol{p}}_\perp^2}{2m_e} + \omega_L\hat{L}_z + \frac{1}{2}m_e\omega_L^2r^2 \end{aligned} \tag{7}$$

where we have used $k = \frac{p}{\hbar} = \frac{m_e v}{\hbar}$.

This fact allows us to use the numerical method for TDSE in Quantum Mechanics to deal with the paraxial equation.

Our starting point for the simulation is the dimensionless version of the paraxial equation (using w_m as transverse characteristic scale and z_m as longitudinal scale) in Cartesian coordinates:

$$i\partial_z \Psi = \left[-\frac{1}{4}(\partial_x^2 + \partial_y^2) - i\,(x\partial_y - y\partial_x) + (x^2 + y^2) \right] \Psi \tag{8}$$

With an initial condition at the knife-edge cut position z_k: $\Psi(x, y, z_k)\Theta(y)$, where $\Theta(.)$ is the Heaviside function. And we take the grid length three times larger than the maximum beam width at the knife-edge cut position to have a zero Dirichlet boundry condition.

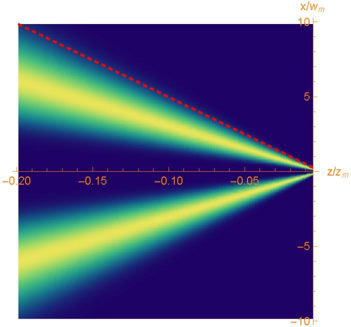

Figure: Cross section of the probability density of the electron beam at $y = 0$.

- The significant variation in transverse scales within the simulation domain requires a fine spatial grid to meet the stability and precision of the simulation.

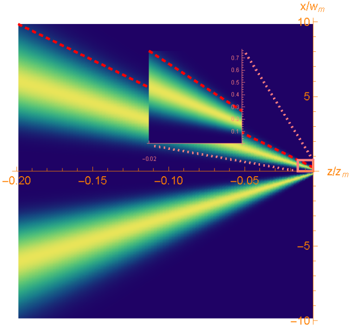

Figure: Cross section of the probability density of the electron beam at $y = 0$, with the part near the observation plane zoomed.

- As an estimate, if we want to have a 100×100 resolution for the intensity profile near the observation plane, then the initial grid should be of size $(100 \times \frac{10}{0.25}) \times (100 \times \frac{10}{0.25}) = 4000 \times 4000$.
- Thus any local discretization for the z-direction is inefficient and will propose a big challenge for the RAM and CPU.
- We use a global approximation for the propagation using the *Chebyshev method*, employed in solving time-dependent Schrödinger equation.

In Quantum Mechanics, for the TDSE $i\hbar\frac{\partial}{\partial t}\psi(\boldsymbol{x},t) = \hat{H}\psi(\boldsymbol{x},t)$, by interpreting it as a first order differential equation in time (that is, ignoring any potential differential operators in $\hat{H}$), there is a formal solution available:

$$\psi(\boldsymbol{x},\Delta t) = e^{-i\hat{H}\Delta t}\psi(\boldsymbol{x},0) = \sum_{n=0}^{\infty}\frac{(-1)^n}{n!}\left(\frac{i\hat{H}\Delta t}{\hbar}\right)^n\psi(\boldsymbol{x},0) \equiv \hat{U}(\Delta t)\psi(\boldsymbol{x},0), \quad (9)$$

where $\psi(\boldsymbol{x},0)$ is the initial condition, and $\hat{U} = e^{-i\hat{H}t/\hbar}$ is the unitary propagation operator.

The Chebysev expansion is a global approximation (i.e., it is valid for any value of Δt), allowing us to calculate the final state of the system directly, given the Hamiltonian and initial state.

It does so by *expanding the unitary propagation operator as a series expansion of Chebyshev polynomials*, unlike the more common power series approach used by the Taylor expansion.

The Chebyshev series expansion of the unitary time propagation operator is given by

$$\psi(\boldsymbol{x}, t+\Delta t) = e^{-i\frac{(E_{\max}+E_{\min})\Delta t}{2\hbar}} \left[J_0(\alpha) T_0(-i\widetilde{H}) + 2\sum_{n=1}^{\infty} J_n(\alpha) T_n(-i\widetilde{H}) \right] \psi(\boldsymbol{x}, t), \qquad (10)$$

where:

- $E_{\min}, E_{\max} \in \mathbb{R}$ are the values we used to normalize the Hamiltonian so that its energy eigenvalues lie in the domain $E \in [-1, 1]$ (this allows maximal convergence of the Chebyshev expansion)
- $\alpha = \frac{(E_{\max}-E_{\min})\Delta t}{2\hbar}$, $J_n(\alpha)$ are the Bessel function of the first kind,
- T_n are the Chebyshev polynomials of the first kind,
- the normalized Hamiltonian is defined as

$$\widetilde{H} = \frac{2\hat{H} - E_{\max} - E_{\min}}{E_{\max} - E_{\min}}$$

The power of the Chebyshev expansion as a global method comes from the Bessel function series coefficients, as it turns out that $J_n(\alpha) \approx 0$ when $n > |\alpha|$, allowing for fast convergence and significantly higher accuracy after only $\lfloor |\alpha| \rfloor$ terms.

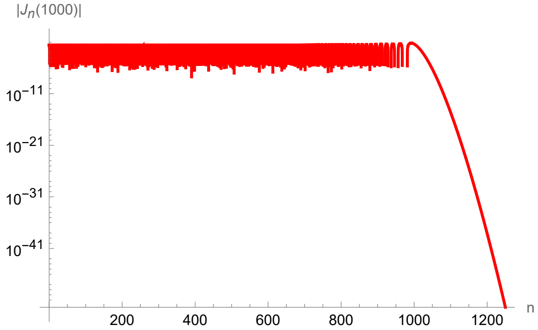

Figure: For fixed α, $|J_n(\alpha)|$ decreases quickly for $n > |\alpha|$

Note that although the Chebyshev polynomials $T_n(.)$ is implemented in most programming languages, we cannot simply make use of it directly, since it only accepts a floating point value x, whereas our argument is $\widetilde{H}$, an operator or a matrix!

Thankfully, the Chebyshev polynomials satisfy a very convenient set of recurrence relations,

$$\begin{aligned} T_0(x) &= 1 \\ T_1(x) &= x \\ T_{n+1}(x) &= 2xT_n(x)T_{n-1}(x), \end{aligned}$$

which generalise in the case of operator arguments:

$$\begin{aligned} T_0(-i\widetilde{H})\psi(\boldsymbol{x},t) &= \psi(\boldsymbol{x},t) \\ T_1(-i\widetilde{H})\psi(\boldsymbol{x},t) &= -i\widetilde{H}\psi(\boldsymbol{x},t) \\ T_{n+1}(-i\widetilde{H})\psi(\boldsymbol{x},t) &= -2i\widetilde{H}T_n(-i\widetilde{H})\psi(\boldsymbol{x},t)T_{n-1}(-i\widetilde{H})\psi(\boldsymbol{x},t). \end{aligned}$$

For the dimensionless version of the paraxial equation:

$$i\partial_z \Psi = \left[-\frac{1}{4}(\partial_x^2 + \partial_y^2) - i\,(x\partial_y - y\partial_x) + (x^2 + y^2) \right] \Psi \tag{11}$$

We can simply replace the Δt to Δz, setting $\hbar = 1$ and take the effective Hamiltonian as

$$H_{\text{eff}} = -\frac{1}{4}(\partial_x^2 + \partial_y^2) - i\,(x\partial_y - y\partial_x) + (x^2 + y^2)$$

And in the following, we show our simulation results, together with a line based on the theoretical prediction.

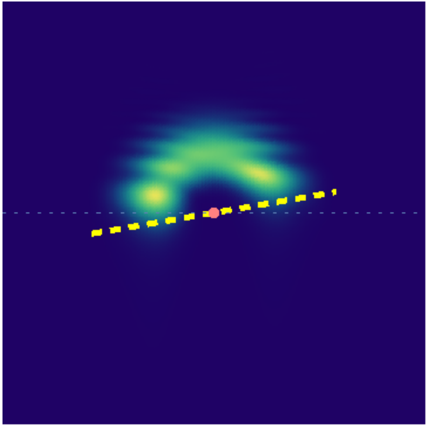

Figure: Simulation result of the propagation, $n = 0, \ell = 3, z_k = -20\ \mu\mathrm{m}$

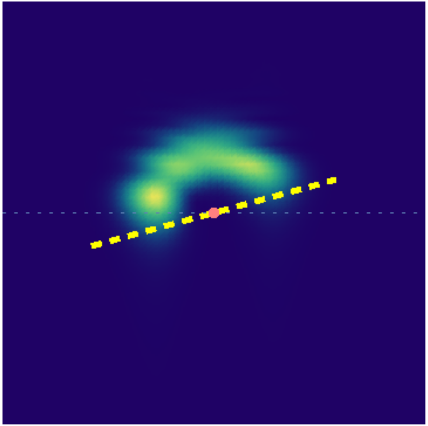

Figure: Simulation result of the propagation, $n = 0, \ell = 3, z_k = -50\ \mu\mathrm{m}$

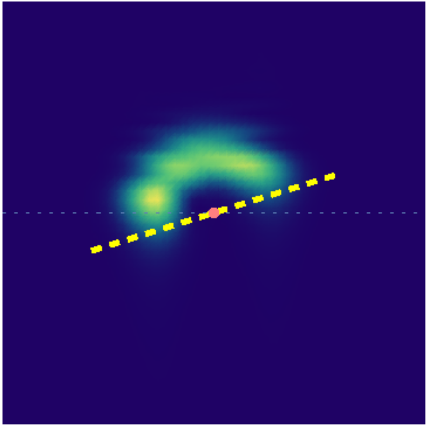

Figure: Simulation result of the propagation, $n = 0, \ell = 3, z_k = -80\ \mu\mathrm{m}$

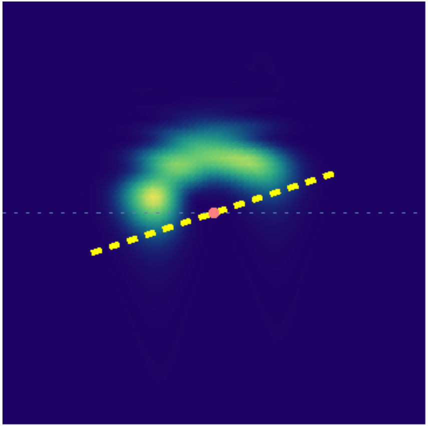

Figure: Simulation result of the propagation, $n = 0, \ell = 3, z_k = -100\ \mu\mathrm{m}$

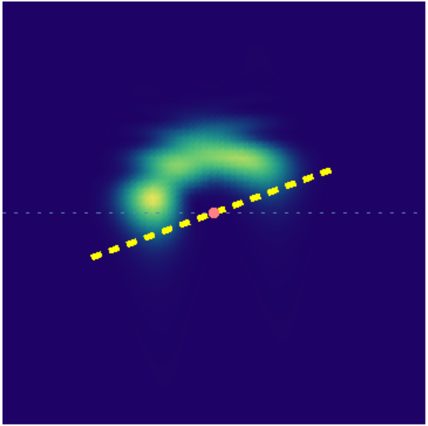

Figure: Simulation result of the propagation, $n = 0, \ell = 3, z_k = -150\ \mu\mathrm{m}$

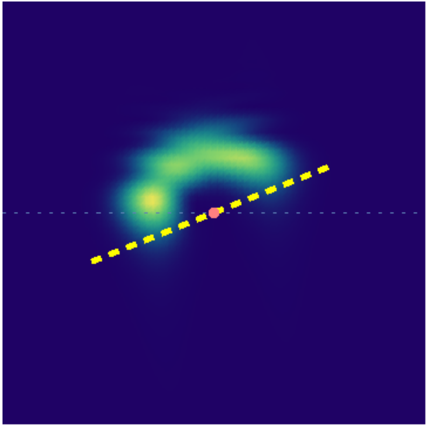

Figure: Simulation result of the propagation, $n = 0, \ell = 3, z_k = -200\ \mu\mathrm{m}$

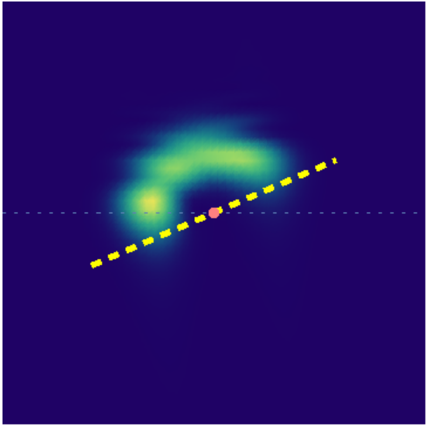

Figure: Simulation result of the propagation, $n = 0, \ell = 3, z_k = -250\ \mu\text{m}$

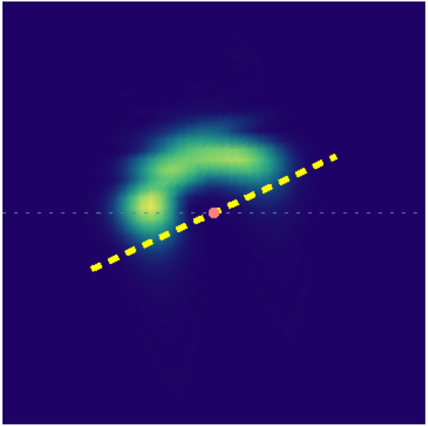

Figure: Simulation result of the propagation, $n = 0, \ell = 3, z_k = -300\ \mu\text{m}$

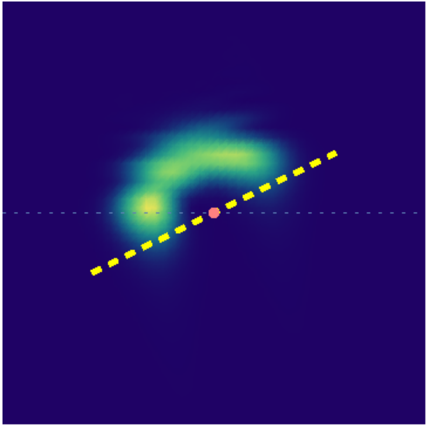

Figure: Simulation result of the propagation, $n = 0, \ell = 3, z_k = -350\ \mu\mathrm{m}$

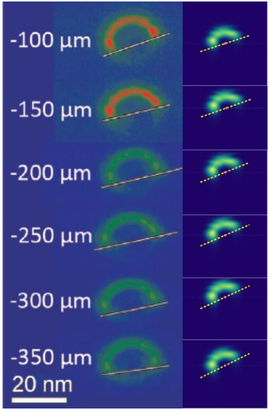

Figure: Comparison with the intensity profile observed in the experiment in (Schachinger et al. 2015)

Conclusion

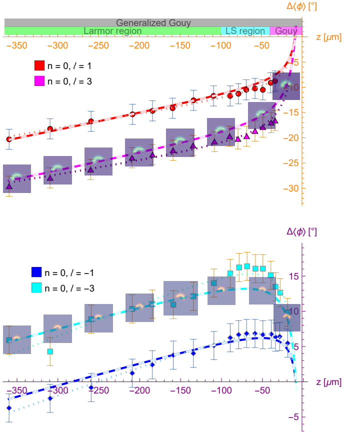

- Our work can be summarised in a figure, with both the conceptually imposed Generalized Gouy Rotation based on the paraxial Landau modes, the fitting of experimental data and the simulation under the experimental settings with the Chebyshev method.

Conclusion

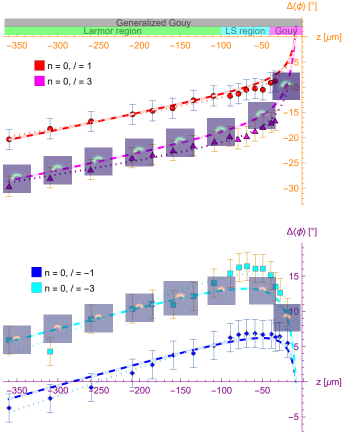

- Our work can be summarised in a figure, with both the conceptually imposed Generalized Gouy Rotation based on the paraxial Landau modes, the fitting of experimental data and the simulation under the experimental settings with the Chebyshev method.
- To check further the validity of the model based on paraxial Landau modes, experiments can be done for some different parameters so that we can distinguish the beam width from the free beams and Landau states.

Conclusion

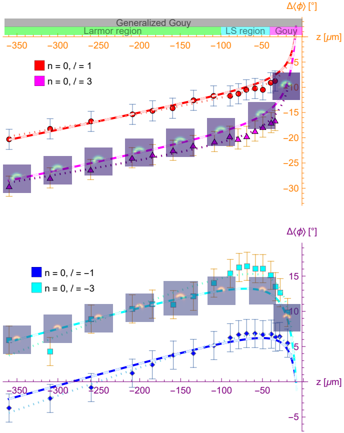

- Our work can be summarised in a figure, with both the conceptually imposed Generalized Gouy Rotation based on the paraxial Landau modes, the fitting of experimental data and the simulation under the experimental settings with the Chebyshev method.
- To check further the validity of the model based on paraxial Landau modes, experiments can be done for some different parameters so that we can distinguish the beam width from the free beams and Landau states.
- The model based on the paraxial Landau modes is still not perfect, there exists some discrepancies, especially for the case of $|\ell| = 3$. This may need models considering higher order corrections or experiment with better precision (e.g., more uniform magnetic field, reduction of knife edge roughness and position measure errors, etc.).

- Bliokh, Konstantin Y. et al. (Nov. 2012). "Electron Vortex Beams in a Magnetic Field: A New Twist on Landau Levels and Aharonov-Bohm States". In: *Phys. Rev. X* 2 (4), p. 041011. DOI: 10.1103/PhysRevX.2.041011.
- Greenshields, Colin R, Sonja Franke-Arnold, and Robert L Stamps (Sept. 2015). "Parallel axis theorem for free-space electron wavefunctions". In: *New Journal of Physics* 17.9, p. 093015. DOI: 10.1088/1367-2630/17/9/093015.
- Guzzinati, Giulio et al. (Feb. 2013). "Observation of the Larmor and Gouy Rotations with Electron Vortex Beams". In: *Phys. Rev. Lett.* 110 (9), p. 093601. DOI: 10.1103/PhysRevLett.110.093601.
- Melkani, Abhijeet and S. J. van Enk (July 2021). "Electron vortex beams in nonuniform magnetic fields". In: *Physical Review Research* 3.3. DOI: 10.1103/physrevresearch.3.033060.
- Schachinger, T. et al. (Nov. 2015). "Peculiar rotation of electron vortex beams". In: *Ultramicroscopy* 158, pp. 17–25. DOI: 10.1016/j.ultramic.2015.06.004.

Schattschneider, P. et al. (Aug. 2014). "Imaging the dynamics of free-electron Landau states". In: *Nature Communications* 5.1, p. 4586. DOI: 10.1038/ncomms5586.

Zou, Liping, Pengming Zhang, and Alexander J. Silenko (Jan. 2021). "General quantum-mechanical solution for twisted electrons in a uniform magnetic field". In: *Phys. Rev. A* 103 (1), p. L010201. DOI: 10.1103/PhysRevA.103.L010201.

Thanks for your attention!